Journal of Power Sources 410–411 (2019) 124–131

Contents lists available at ScienceDirect

Journal of Power Sources

journal homepage: www.elsevier.com/locate/jpowsour

Temperature dependent electrochemical performance of graphite anodes for K-ion and Li-ion batteries

Ryan A. Adams, Arvind Varma, Vilas G. Pol*

Davidson School of Chemical Engineering, Purdue University, 480 Stadium Mall Dr., West Lafayette, IN, 47907, United States

HIGHLIGHTS

- Graphite anode was analyzed across temperatures for Li-ion and K-ion batteries.
- K-ion batteries had poor kinetics, high polarization, and significant ageing.
- The K metal counter electrode limits the half-cell performance of K-ion batteries.
- A Prussian blue – graphite K-ion full cell showed enhanced rate capability.

ARTICLE INFO

Keywords:
Potassium ion battery
Graphite anode
Lithium ion battery
Thermal behavior

ABSTRACT

The electrochemical behavior of graphite anode for potassium-ion batteries (KIBs) is investigated in detail over varying operating temperatures (0–40 °C) with comparisons made to lithium-ion batteries (LIBs). Three main categories of cell performance are analyzed and evaluated, namely, kinetics, aging, and polarization. At 10 °C and below, the KIBs exhibit poor rate capability, which can be attributed to the decreased solid-state diffusion coefficient, and the amplified charge-transfer and SEI resistances. In comparison to LIBs, KIBs exhibit rapid cell aging at elevated temperatures, owing to augmented SEI growth induced by the significant volumetric change of graphite during potassiation. 3-electrode cell studies reveal the dramatic polarization of K metal at 0 °C (161 mV), while the extreme reactivity of K metal causes a severe rise in impedance from cell storage at 50 °C. A full cell system comprising Prussian blue cathode and graphite anode is evaluated, which removes the issues associated with the K metal counter electrode and enhances rate performance at 0 °C. These findings provide a thorough basis for understanding the temperature dependent behavior of graphite anode for KIBs and its performance concerns at low and elevated temperatures.

1. Introduction

Rechargeable lithium-ion batteries (LIBs) are currently the dominant electrical energy storage technology with widespread usage in portable electronics and electric vehicles due to their high energy density and reasonable lifetime. However, the scarcity and poor distribution of Li resources limit the scalability of this technology proceeding into the future, especially for large scale applications, such as grid storage of renewable energy (e.g. solar and wind) [1,2]. While efforts have been made towards the recovery of valuable cobalt and lithium resources from spent LIBs, the economics and complexity of these recycling processes limit their viability [3,4]. Thus, researchers have become interested in alternative alkali metal-ion chemistries, replacing Li with Na, and more recently K, for applications where kWh $\$^{-1}$ is more important than energy density [5–7]. These batteries operate with an analogous mechanism to LIBs, with intercalation storage between cathode and anode in a non-aqueous electrolyte. Despite its larger cationic size, potassium-ion batteries (KIBs) have some intrinsic advantages over sodium-ion batteries (NIBs), including a higher operating voltage and increased electrolyte transference number in organic solvents due to the weaker Lewis acidity of K^+ [8,9]. A variety of electrode materials have been explored for KIBs, with promising cathodes including layered metal oxides ($K_{0.3}MnO_2$, $K_{0.7}Fe_{0.5}Mn_{0.5}O_2$, $K_{0.6}CoO_2$) [10–12], polyanionic compounds ($KVPO_4F$ and $KVOPO_4$) [13], and hexacyanoferrates (Prussian blue, $K_{1.89}Mn[Fe(CN)_6]_{0.92}{\cdot}0.75H_2O$) [14–16]. For the anode side, graphitic and carbonaceous materials are the most viable choices, including hard carbon microspheres, N-doped carbon nanofibers, tire-derived carbon, soft carbon nanorods as well as MXenes [17–21].

The key advantage of KIBs over NIBs comes from the ability of

* Corresponding author.
E-mail address: vpol@purdue.edu (V.G. Pol).

https://doi.org/10.1016/j.jpowsour.2018.11.007
Received 22 August 2018; Received in revised form 19 October 2018; Accepted 3 November 2018
0378-7753/ © 2018 Elsevier B.V. All rights reserved.

graphite to reversibly intercalate K^+ to a stage-one KC_8 structure (279 mAh g^{-1}), whereas Na^+ is limited to a stage-eight NaC_{64} structure (35 mAh g^{-1}) [22–24]. Commercial LIBs have primarily used graphite as anode for over two decades, due to its good cycling stability, favorable low voltage profile, high tap density (as compared to non-graphitic carbons), low first cycle inefficiency, and reasonable reversible capacity. In fact, the main hurdle to NIB commercialization comes from the lack of a suitable anode material, where the front-runner hard carbon materials suffer from poor first cycle Coulombic efficiency and long-term cycling stability [25]. Intercalation of K^+ into graphite is mechanistically similar to that of Li^+, with multiple phase changes occurring from stage-three KC_{36} → stage-two KC_{24} → stage-one KC_8 structures, resulting in voltage plateaus near 0.2 V (vs. K/K^+) [23]. The slightly higher average voltage for K^+ insertion into graphite, as compared to Li^+, is beneficial in preventing K metal plating and dendrite growth under high current or low temperature conditions, which is a severe safety concern. Due to the bulkier size of K^+ as compared to Li^+, a larger volumetric expansion of 61% occurs upon full potassiation (vs. 11% for lithiation); however, full reversibility of this intercalation process has been demonstrated without graphene exfoliation [23,24]. Cell optimization of electrode binder, such as functionalized sodium carboxymethyl cellulose (CMCNa), and electrolyte have significantly improved the first cycle Coulombic efficiency and long-term cycling stability, despite the large volumetric expansion [24,26].

With KIB research still in its infancy, there remain many challenges and unexplored aspects that require further investigation to evaluate the viability of this chemistry for commercialization. For example, the effect of operating temperature on KIB performance remains completely unknown, where all experimental studies thus far have been conducted at room temperature only. It is well known that operating temperature plays a significant role in LIB performance, lifetime, and safety [27]. At low temperatures (< 10 °C), reduced energy and power capability result from the sluggish kinetics, with severe safety concerns arising from possible Li metal plating and dendrite formation on the graphite anode at high currents [28,29]. At elevated temperatures (> 40 °C), accelerated battery aging occurs due to irreversible solid electrolyte interphase (SEI) growth [30,31]. Additionally, thermal runaway remains a significant issue for LIBs, where the metastable electrode materials and flammable organic electrolyte result in self-propagated cell combustion at extreme temperatures (> 80 °C) [32]. Recently, we investigated the thermal runaway behavior of graphite anode in KIBs via differential scanning calorimetry, where exothermic reactions of K_xC_8 – electrolyte initiate as early as 100 °C, with a strong dependence on state of charge, cycle number, electrode binder, and graphite surface area [33]. This illustrates the need to evaluate the KIB graphite anode system over a wide operating temperature range, and to determine the effects of temperature on battery performance, aging, and safety.

In this study, we conducted thorough electrochemical evaluation of graphite anode for KIBs and LIBs to compare their behavior across a wide temperature range (0–40 °C). Three major parameters were evaluated: (1) diffusion kinetics and rate capability, (2) cell aging and impedance growth, and (3) cell polarization. Coin cells were constructed using analogous electrolytes ($LiPF_6$/KPF_6 salt dissolved in a mixed carbonate solvent), with the non-idealities of the K metal reference/counter electrode determined via 3-electrode cell and full cell studies. Through this work, we aim to provide further mechanistic insight into K^+ - graphite intercalation electrochemistry and its differences with the well-known Li system.

2. Experimental

To facilitate comparisons between chemistries, the same graphite electrode was utilized for K-ion and Li-ion battery testing, comprising of 80 wt. % synthetic graphite (MTI Corp), 10 wt. % conductive additive (Super P carbon black), and 10 wt. % CMCNa binder (Sigma-Aldrich). Material characterization for this standard graphite powder can be found in our prior related work [33]. These materials were mixed in a slurry utilizing water as solvent for 30 minutes and cast onto copper foil (MTI Corp) prior to drying in a vacuum oven at 80 °C for 12 hours. For coin cell testing, 12 mm diameter electrodes were punched out with an average graphite loading of 2 mg cm^{-2}. Electrochemical testing was performed in coin-type 2032 half-cells, with Li (MTI Corp) or K metal (Sigma-Aldrich) foils used as reference and counter electrode. 3-electrode cells were constructed using the methodology of Juarez-Robles et al., albeit with Li or K metal as the reference electrode [34]. Glass microfiber (Whatman 934-AH) was utilized as separator, while the electrolyte was 1 M $LiPF_6$ in ethylene carbonate (EC):diethyl carbonate (DEC) (1:1 volumetric ratio) for LIBs and 0.8 M KPF_6 in EC:DEC (1:1) for KIBs (all salts and solvents obtained from Sigma-Aldrich).

Galvanostatic cycling was performed via an Arbin cycler with cells contained in an ESPEC environmental chamber for temperature control, with five temperatures chosen for analysis: 0 °C, 10 °C, 22 °C, 30 °C, and 40 °C. Due to the low melting temperature of K metal (63.5 °C), the thermal analysis of cells was conducted at a maximum temperature of 40 °C for safety. Cycling was performed in the voltage range of 0.01–1.5 V (vs. Li/Li^+ or K/K^+) with specific currents provided in terms of mA g^{-1}. Galvanostatic intermittent titration technique was conducted with 30-min pulses at C/10 (1C = 372 mA g^{-1} for LIBs & 1C = 279 mA g^{-1} for KIBs) and 1-h relaxations between pulses. Potentiostatic electrochemical impedance spectroscopy (EIS) was performed with a Gamry-600 + instrument, in the frequency range of 0.01–10^6 Hz, with an amplitude of 5 mV and prior cell conditioning to a voltage of 200 mV (LIBs) or 500 mV (KIBs). EIS spectra were fit using Echem Analyst software from Gamry Instruments. To analyze battery self-discharge and aging, cells conditioned at 22 °C were discharged (i.e. lithiated/potassiated), stored at 50 °C for 1 week at open circuit voltage (OCV), and then cycled at room temperature again, with EIS collected before and after storage at 50 °C.

3. Results and discussion

3.1. Kinetics

To analyze the effect of temperature on kinetics, an initial inquiry was conducted via galvanostatic cycling at various specific currents (20–500 mA g^{-1}), with obtained charge capacities shown in Fig. 1a for Li and Fig. 1b for K. At 22 °C, both chemistries achieve their theoretical capacities of 279 mAh g^{-1} and 372 mAh g^{-1} for K and Li respectively, after initial cell conditioning and SEI formation. At higher temperatures, the theoretical capacity of 372 mAh g^{-1} is exceeded for LIBs, likely due to the storage of Li^+ in Super P carbon black, as previously observed [35]. Due to the low surface area (3.4 m^2 g^{-1}), larger particle diameters, and limited diffusion of K^+/Li^+ through the edge of the graphene sheets, both chemistries suffer from poor rate capability at higher currents of 500 mA g^{-1} [33]. As expected, increased temperatures augment the capacity achieved for LIBs, from 100 mAh g^{-1} (22 °C) to 300 mAh g^{-1} (40 °C) at 500 mA g^{-1}, while decreased temperatures lower the capacity dramatically. In comparison, graphite anode for KIB shows less improvement at elevated temperatures, and already starts failing at moderate currents by 10 °C.

To provide further insight into the kinetic limitations at 0 °C, a coin cell was discharged fully (i.e. lithiated or potassiated) at 22 °C after 5 conditioning cycles, and subsequently charged (i.e. delithiated or depotassiated) at 0 °C or 22 °C as shown in Fig. 1c. Both systems obtain nearly the full capacity upon charging at 0 °C, indicating that the rate limiting step involves insertion of the alkali ion into graphite, rather than extraction, agreeing with previous observations for LIBs [36]. However, the hysteresis between the charge voltage curves at 0 °C and 22 °C is significantly higher for the KIB. Additionally, the charge profiles for both systems at 0 °C display an initial overpotential hump, likely due to a charge-transfer related activation energy barrier amplified by the low temperature [37]. As shown in Fig. 1c, the poor rate

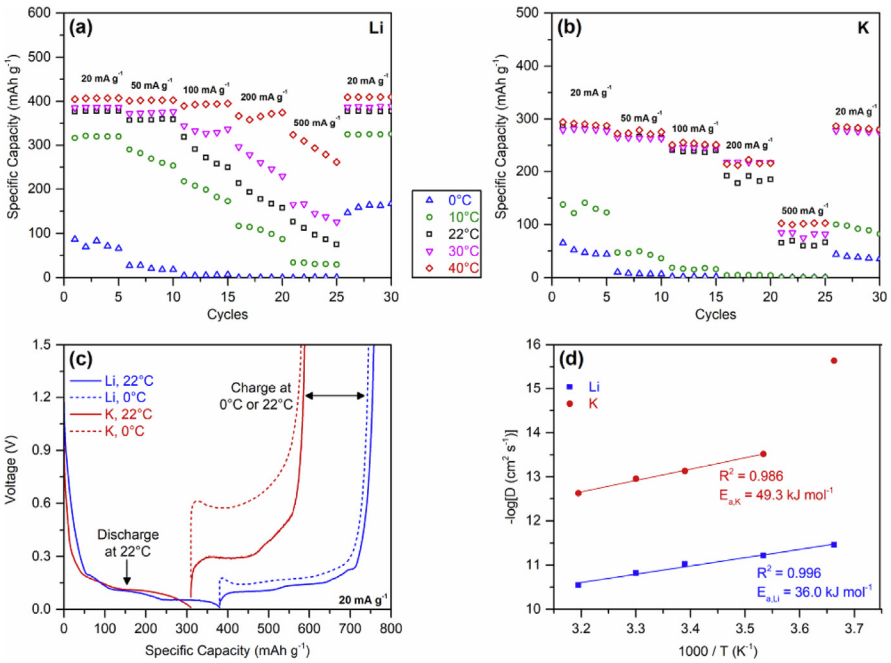


Fig. 1. Kinetic analysis of graphite across temperatures. (a) Charge capacity of Li at various specific currents. (b) Charge capacity of K at various specific currents. (c) Voltage profile for discharge at 22 °C with subsequent charge at 0 °C or 22 °C, at 20 mA g^{-1} and cycle 5. (d) Solid-state diffusion coefficients of Li^+ and K^+ in graphite from 0 to 40 °C, with calculated diffusion activation energies determined by the Arrhenius equation.

capability at low temperatures could originate from several factors, such as cell polarization, diffusional resistance, or poor charge-transfer kinetics. Evaluation of both electrolyte compositions indicates that no freezing or salt precipitation occurs at 0 °C (Table S1).

To determine the source of these kinetic limitations, the diffusion coefficients of Li^+ and K^+ in graphite were determined as a function of temperature, using the method of Kulova et al. (experimental details in Supporting Information) [38,39]. The calculated diffusion coefficients are shown in Fig. 1d, where D_{Li^+} is in the range of 10^{-11} cm^2 s^{-1}, agreeing well with previously calculated values [40]. As expected, the diffusion coefficient observes an Arrhenius relationship with temperature as follows,

$$D = D_0 \, exp\left(-\frac{E_A}{RT}\right)$$

where E_A is the activation energy for cation diffusion in graphite. An activation energy of 36.0 kJ mol^{-1} is obtained for Li^+, showing a good linear fit and matching previously obtained values [39]. Contrarily, the diffusion coefficient for K^+ is on the order of 10^{-13} cm^2 s^{-1}, indicating much more sluggish solid-state diffusion, as expected from the larger cationic size of K^+ and the poor observed rate capability. A linear trend is also observed for D_{K^+}, with an activation energy of 49.3 kJ mol^{-1}, ignoring the data point at 0 °C, which has a significantly lower diffusion coefficient value of 10^{-16} cm^2 s^{-1}. Much lower specific currents were required to achieve a linear response at 0 °C (even using a 3-electrode cell), with extreme polarization preventing cell operation. Interestingly, first-principles calculations have predicted decreased site jump energy barriers for K^+ as compared to Li^+, suggesting that larger cations should diffuse more smoothly in graphite, suggesting a discrepancy between experimental and computational results [41].

To investigate this inconsistency, EIS analysis was utilized to probe and compare the impedance of the two battery chemistries. To determine the effect of temperature, EIS was performed on well-conditioned cells (C/10 for 10 cycles at 22 °C) at a specified state-of-charge (200 mV for Li, 500 mV for K) in an environmental chamber for temperature control. The spectra are displayed in Fig. 2a for Li and Fig. 2b for K, with insets for the high frequency region. Both systems demonstrate a strong relationship of impedance with temperature, albeit K even more so, with increasing temperature lowering cell impedance as expected [42]. Both sets of spectra include several overlapping semicircles, which can be ascribed to SEI layer resistance and capacitance (at high frequencies), as well as a Randles circuit for charge-transfer resistance and double layer capacitance (at medium frequencies). Additionally, a linear region of 45° at low frequencies is observed representing solid-state diffusion impedance via a Warburg element. The equivalent circuit utilized to fit the EIS data is shown in Figure S5, where constant phase elements (CPEs) are used for modeling to improve the fitting, which physically arises from inhomogeneities in the particle surface.

After fitting, the values corresponding to charge-transfer and SEI resistance are plotted in Fig. 2c and d, respectively, with additional fitting parameters listed in Tables S2-3. An Arrhenius relationship is observed for charge-transfer resistance, with calculated activation energies of 80.8 kJ mol^{-1} for K and 51.7 kJ mol^{-1} for Li, which agrees well with prior obtained values for LIBs [42–44]. The impedance of KIBs is significantly higher than that of LIBs, which suggests that the augmented energy barrier caused by insertion of a larger cation is a stronger effect than the beneficial weaker Lewis acidity of K^+ [26]. The SEI resistances also follow Arrhenius relationships, with activation energies of 77.9 kJ mol^{-1} for K and 53.8 kJ mol^{-1} for Li. While the properties of the KIB SEI layer remain largely undetermined, it was shown that K^+ possesses low ionic conductivity within the SEI as compared to Li^+, resulting in significant overpotentials [45]. Additionally, SEI surface films consisting on ionic Na compounds are much more resistive than those comprised of ionic Li compounds, with the trend continuing for the soft K cations due to the resulting formation of less compact and ionically conductive compounds [46]. Computational studies have predicted a disordered and flexible solvation structure for K^+ in ethylene carbonate, enabling easier electrode – electrolyte migration than with the well-defined Li^+ solvation shell, meaning this discrepancy in rate behavior likely arises from sluggish transport through the KIB SEI layer [47]. Since this EIS was conducted with half-cells, SEI from the metal counter electrodes will also contribute to the measured impedance. Due to the increased reactivity of K metal over Li metal, it is likely that K metal will have increased SEI formation and impedance, and that its composition may vary across temperatures. The influence of the counter electrode will be discussed in further detail later.

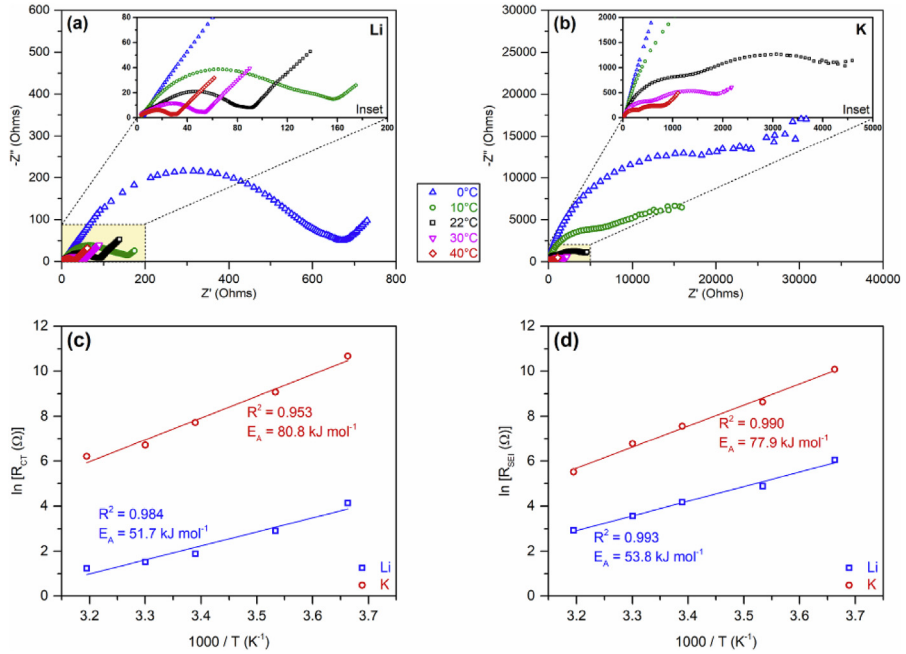


Fig. 2. Dependence of cell impedance with temperature. Nyquist plots of electrochemical impedance spectra conducted at various temperatures for (a) Li at 200 mV and (b) K at 500 mV. (c) Charge-transfer resistance and (d) SEI resistance, with corresponding activation energies determined by the Arrhenius equation.

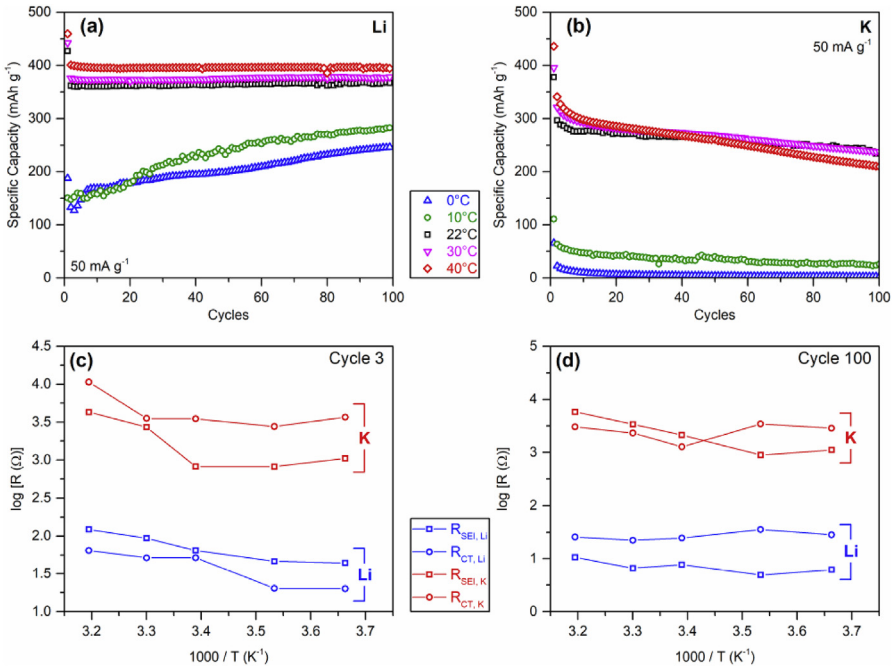


Fig. 3. Cell aging dependence on operating temperature. (a) Discharge capacity of LIB cycled at 50 mA g^{-1}. (b) Discharge capacity of KIB cycled at 50 mA g^{-1}. Aging of cells conditioned at various temperatures, with subsequent electrochemical impedance spectroscopy analysis conducted at 22 °C. (c) SEI and charge-transfer resistances after 3 slow formation cycles conducted at 5 mA g^{-1} (d) SEI and charge-transfer resistances after 100 cycles at 50 mA g^{-1}.

3.2. Aging

Besides affecting kinetic parameters, extreme operating temperatures can significantly increase the rate of cell degradation and aging. For an initial probe into the effect of temperature on aging, long term galvanostatic cycling was conducted at 50 mA g^{-1} over the range of 0–40 °C, with discharge capacities shown in Fig. 3a (Li) and Fig. 3b (K). For LIBs, stable capacities are observed from 22 to 40 °C, with minor increases in capacity values for the higher temperatures. The lower temperatures display an increase in capacity over cycle number, likely due to material activation or improving electrolyte-electrode contact over time [48]. In contrast, KIBs exhibit a slight capacity fade with cycling, due to the 61% volumetric expansion during potassiation. The rate of this capacity fade increases with temperature, arising from augmented SEI growth on exposed graphite caused by SEI cracking during repeated material expansion and contraction. The average capacity loss per cycle is 0.167% for 22 °C, 0.236% for 30 °C, and 0.390% for 40 °C. The lower temperatures give minimal capacity, agreeing well with the prior rate study in Fig. 1b, and do not activate over time in contrast to LIBs, indicating that the high cell impedance results in nominal capacity. The Coulombic efficiencies for the initial cycles are shown in Figure S6, where both chemistries show the greatest stability at room temperature, with excessive SEI growth at elevated temperatures and possible alkali metal plating at lower temperatures. Additionally, LIBs stabilize in Coulombic efficiency across all temperatures more quickly, plateauing by cycle 15, as compared to cycle 25 for KIBs.

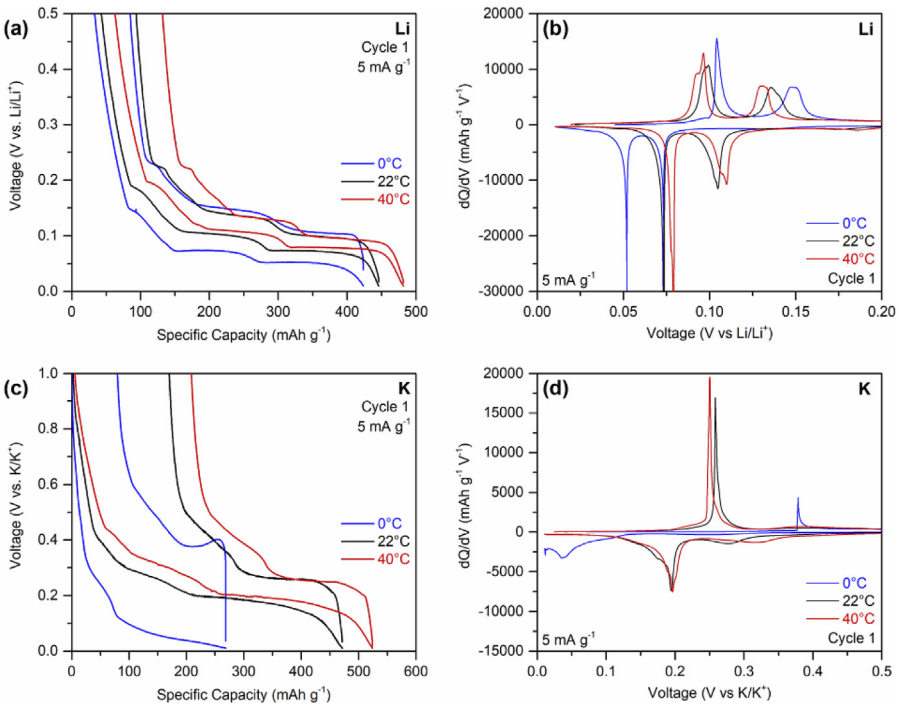


Fig. 4. First cycle charge-discharge voltage profile variation with temperature. (a) Voltage profile for LIB at 0 °C, 22 °C, and 40 °C at 5 mA g^{-1}, and corresponding (b) differential capacity plot of LIB voltage profile. (c) Voltage profile for KIB at 0 °C, 22 °C, and 40 °C at 5 mA g^{-1}, and corresponding (d) differential capacity plot of KIB voltage profile.

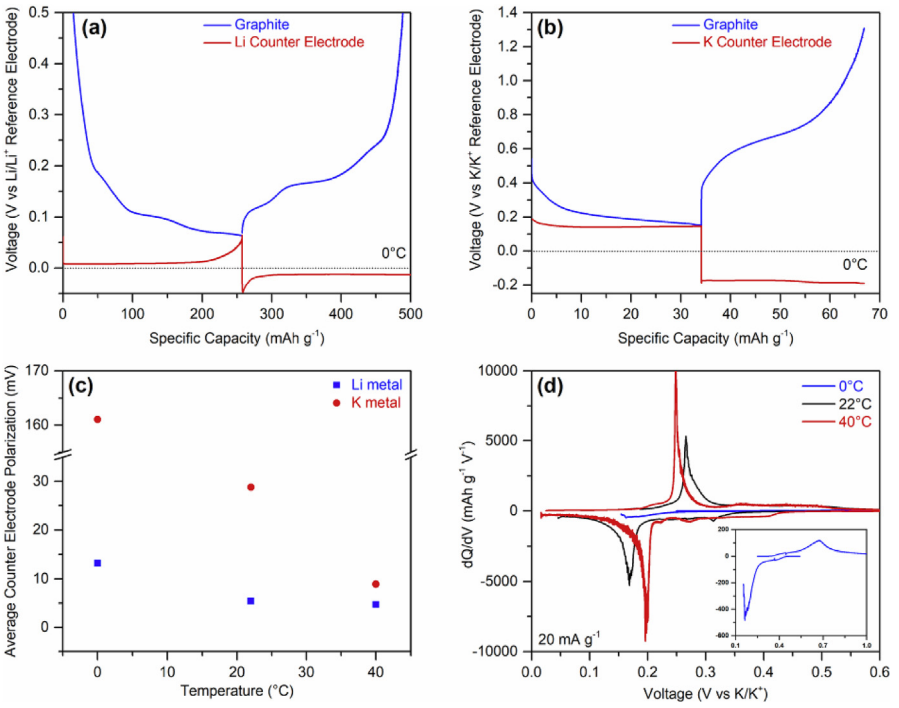


Fig. 5. Polarization of the alkali metal counter electrode. (a) Voltage profile of 3-electrode LIB cell at 20 mA g^{-1} and 0 °C. (b) Voltage profile of 3-electrode KIB cell at 20 mA g^{-1} and 0 °C. (c) Dependence of the average alkali metal counter electrode polarization with temperature. (d) Differential capacity plot of the graphite voltage profile across temperatures in a 3-electrode KIB cell.

To elucidate the aging mechanisms of the batteries more clearly, EIS analysis was conducted at 22 °C, to study the change in impedance for cells previously conditioned at varying temperatures. EIS was conducted for conditioned cells (three slow cycles at 5 mA g^{-1}), as well as cells that had undergone extended cycling (100 cycles at 50 mA g^{-1}) to determine the evolution of impedance over cycling, with spectra displayed in Figures S7-8. All spectra were fit to an equivalent circuit (Figures S5), with the values for charge-transfer and SEI resistance shown in Fig. 3c (three cycles) and Fig. 3d (100 cycles), and additional fitting parameters listed in Tables S4-7. After three slow conditioning cycles, LIBs increase in SEI resistance with cycling temperature from 44.1 Ω at 0 °C to 122.2 Ω at 40 °C, due to the enhanced SEI formation kinetics. In comparison, the KIBs exhibit similar SEI resistance from 0 to 22 °C, but have a significant increase at elevated temperatures, with 820.5 Ω at 22 °C, 2708 Ω at 30 °C, and 4275 Ω at 40 °C, indicating the augmented SEI growth and its poor stabilization. The charge-transfer resistances increase with temperature for both chemistries, likely arising from changes in electrolyte-electrode interfacial contact and the SEI composition and thickness [49]. Overall, slow conditioning suggests that the impedance is directly related to the cycling temperature of the cells, with increased temperature detrimental to electrochemical performance.

After extended cycling, the LIB charge-transfer resistances are independent of temperature, with any slight variation likely arising from

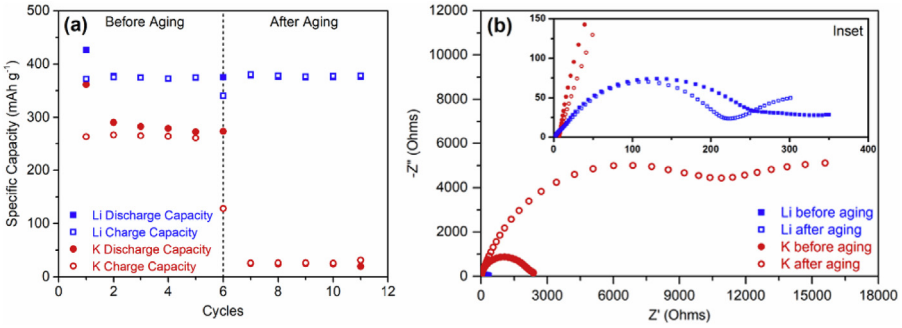


Fig. 6. Cell aging from high temperature storage. (a) Specific capacity before and after aging, at 50 mA g^{-1} and 22 °C. Aging was performed in the middle of cycle 6 at 50 °C for 7 days for fully lithiated/potassiated (discharged) batteries under open circuit voltage. (b) Nyquist plots for electrochemical impedance spectra immediately before and after aging.

cell to cell discrepancies, agreeing with previous results [50]. While there is a slight increase in SEI resistance with cycling temperature, from 7.7 Ω at 22 °C to 10.6 Ω at 40 °C, the system exhibits relatively minor changes as expected of the stable LIB graphite anode. Since the cycling was conducted at a low specific current of 50 mA g^{-1}, the extent of Li plating on graphite should not be significant, which agrees with the small increase in SEI resistance of 4.8 Ω–6.2 Ω, from 10 °C to 0 °C, respectively [51]. In contrast, the KIB SEI resistance increases dramatically with temperature, from 2121 Ω at 22 °C to 5792 Ω at 40 °C, reflecting the accelerated capacity fade during cycling at 40 °C in Fig. 3b. Xiao et al. demonstrated that the 0.8 M KPF_6 EC/DEC electrolyte utilized in this study exhibits poor Coulombic efficiency for reversible plating/stripping of K on Cu substrate, due to poor SEI stabilization on the K metal [52]. The minimum value for SEI resistance is observed after 10 °C cycling, with 0 °C likely resulting in K metal plating. The charge-transfer resistance for KIBs is the lowest at 22 °C, reflecting its optimal electrochemical performance and stability, with higher temperatures augmenting SEI growth and lower temperatures resulting in cell polarization. In comparison, LIBs exhibit a wider optimal operating range of 22–40 °C and still function at lower temperatures, showing the practicality and flexibility of LIBs over KIBs.

3.3. Polarization

The effect of operating temperature on the voltage profile of graphite anode was probed via slow galvanostatic cycling (5 mA g^{-1}) at temperatures of 0 °C, 22 °C, and 40 °C, with the first charge-discharge cycle shown in Fig. 4a (Li) and Fig. 4c (K). Typical voltage profiles are observed, with several plateaus due to phase changes between different staging structures at ~0.1 V for Li^+ and ~0.23 V for K^+. First cycle inefficiencies caused by SEI formation have values of 15%, 16%, and 22% for LIBs at 0 °C, 22 °C, and 40 °C, respectively. In comparison, the first cycle for KIBs have inefficiencies of 28%, 35%, and 39% at 0 °C, 22 °C, and 40 °C, respectively. While both chemistries have augmented SEI formation at higher temperatures, due to enhanced reaction kinetics, LIBs display less variation due to its greater SEI stability across temperatures and the decreased reactivity of Li metal as compared to K metal. Differential capacity curves were generated for these voltage profiles to elucidate the redox peak locations and the hysteresis between charge and discharge processes, as shown in Fig. 4b (Li) and Fig. 4d (K). As expected, the voltage hysteresis increases at lower temperatures due to higher cell impedance, resulting in poorer energy efficiency. This is much more apparent in the KIB profile, with its significant hysteresis of 343 mV between the corresponding reduction and oxidation peaks at 0 °C, as compared to 52 mV for Li. In fact, even at 5 mA g^{-1}, the full theoretical capacity is not achieved at 0 °C, with the potassiation peak interrupted by the lower voltage limit of 0.01 V (vs. K/K^+). This severe polarization contributes significantly to the poor rate performance observed before; however, it is unsure whether this polarization arises from the graphite working electrode or the K metal counter electrode.

3-electrode cells were constructed for each battery chemistry to quantify the polarization originating from the alkali metal counter electrode. The deconvoluted voltage profiles for the graphite anode and alkali metal counter electrode, after prior conditioning for 5 cycles, are shown in Fig. 5a (Li) and Fig. 5b (K) for 0 °C at 20 mA g^{-1}. The corresponding voltage profiles at 22 °C and 40 °C are shown in Figures S9. Noticeably, the Li metal has minimal polarization at 0 °C, with a sharp increase occurring only after the graphite is mostly lithiated. In contrast, the K metal has consistently high polarization across the entire state-of-charge, ending the discharge step after only 35 mAh g^{-1}. The average alkali metal counter electrode polarization was calculated across the three tested temperatures and plotted in Fig. 5c. The Li metal shows relatively low variation from 0 to 40 °C, indicating its suitability as a reference electrode for half-cell testing. In contrast, there was a dramatic decrease in polarization from 0 °C (161 mV) to 40 °C (8.9 mV) for K metal, reflecting the higher activation energy calculated for SEI resistance in KIBs. In agreement with our results, Hess demonstrated the strong effect the cation has on the SEI overpotential, with its nonlinear behavior resulting in enlarged polarization for K at low specific currents as compared to Li [53]. It should be noted that even after neglecting K metal polarization, graphite itself displays a significant hysteresis between the charge-discharge voltage profiles as compared to the LIB case. The differential capacity curves for graphite in the 3-electrode KIB cell at different temperatures are shown in Fig. 5d, where a strong dependence of voltage hysteresis on temperature is observed, reflecting the higher activation energy for KIB charge-transfer resistance.

It is known that K metal is much more reactive than Li, such that it should never be utilized as anode in commercial KIBs for safety reasons. While KIB half-cells have shown promising performance at room temperature, it is unknown how reactive the K metal will be at elevated temperatures in the non-aqueous electrolyte. For safety reasons, an upper limit of 40 °C was chosen for all cycling in this study due to the low melting point (63.5 °C) of K metal. To study this behavior, cell aging was explored for fully discharged half-cells (i.e. lithiated or potassiated) by holding them at 50 °C for a week under OCV. Similar tests have been conducted previously in the literature to analyze the rate of self-discharge and impedance growth for LIBs, albeit usually at higher temperatures, such as 70 °C [54,55]. The charge-discharge capacities before and after aging are shown in Fig. 6a, where all galvanostatic cycling was conducted at room temperature, and the aging process occurred between the discharge and charge steps of the sixth cycle. The LIB shows a minor decrease of 9.4% in charge capacity after aging, which can be attributed to self-discharge, but recovers its full capacity in later cycles, thus indicating the system's stability at 50 °C.

In contrast, the KIB has a significant capacity loss of 53.2% after aging, with a subsequent dramatic decrease in reversible capacity during cycling. The voltage profile for the sixth cycle in Figures S10 reveals the dramatic increase in impedance for the KIB, with the charge plateau occurring at ~1 V instead of ~0.3 V. Additionally, the decreased length of this plateau indicates that the capacity loss in the sixth cycle after aging is likely due to self-discharge. The dramatic rise in impedance after aging, as portrayed by EIS analysis in Fig. 6b,

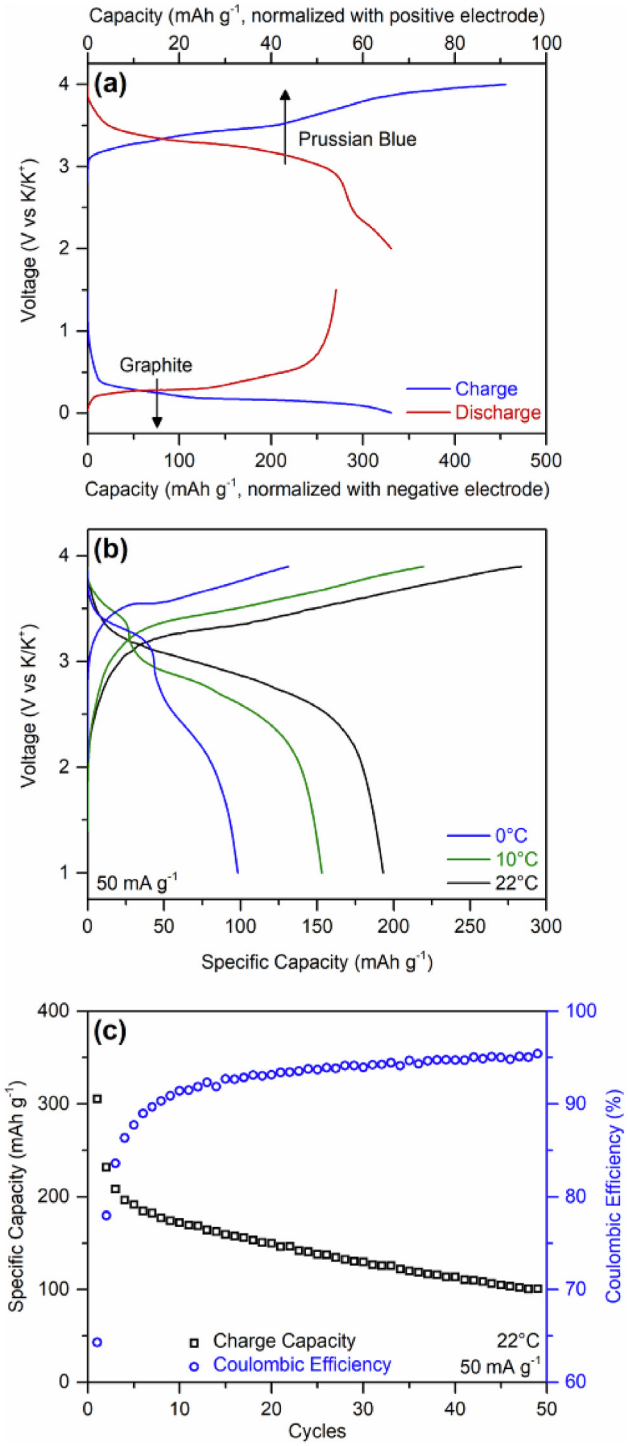


Fig. 7. KIB full cell evaluation. (a) First cycle voltage profiles of Prussian blue cathode and graphite anode half-cells at 50 mA g^{-1}. The capacities are normalized to show the positive to negative charge ratio of the full cell. (b) Full cell charge-discharge voltage profiles across various temperatures from 1.0 to 3.9 V at 50 mA $g^{-1}_{graphite}$. (c) Charge capacities and Coulombic efficiencies for full cell cycling conducted from 1.0 to 3.9 V at 50 mA $g^{-1}_{graphite}$ and 22 °C. Specific current and capacity values in (b) and (c) are normalized by the weight of active material in the graphite anode. (For interpretation of the references to color in this figure legend, the reader is referred to the Web version of this article.)

demonstrates the reactivity of K metal, with augmented SEI formation occurring at 50 °C. Lei et al. showed that DEC solvent is highly reactive in KIBs, and is more electrochemically unstable with K metal than graphite, due to its strong reducibility [56]. Additionally, KPF_6 salt causes a higher voltage hysteresis, due the resulting continuous SEI formation and dendrite growth, when used with K metal [57]. These results indicate that K metal is a poor counter and reference electrode for KIB electrode testing, especially at extreme temperatures where increased polarization and reactivity occur.

3.4. Full cell

In light of these findings, a KIB full cell was constructed utilizing graphite as anode and Prussian blue (PB) nanoparticles as cathode (experimental details in Supporting Information). Material characterization of the synthesized PB cathode (Figures S11) matches well with the prior report, including the crystallinity from X-ray diffraction analysis (JCPDS: 52-1907) [14]. The PB cathode exhibits typical electrochemical behavior in a half-cell, with a specific capacity of 70 mAh g^{-1} resulting from the Fe(II) − Fe(III) redox behavior at ~3.3 V, as seen in Figures S12 [14]. The PB cathode exhibits exceptional rate capability due to its open 3D network, achieving 50 mAh g^{-1} at 200 mA g^{-1} and 40 mAh g^{-1} at 400 mA g^{-1}. Coupled with the high mass ratio of PB to graphite (to achieve 1:1 cathode to anode charge ratio in the full cell), any limitation in rate capability for the full cell system will likely originate from the graphite anode. Additionally, good cycling stability is observed for PB cathode, with minimal capacity loss occurring after 150 cycles at 200 mA g^{-1} (Figures S12d). The first cycle charge-discharge voltage profiles for the PB cathode and graphite anode in the half-cell configuration (prior to disassembly and full cell construction) are shown in Fig. 7a. Both electrodes exhibit initial irreversible capacity loss, due to SEI formation on graphite and decomposition of interstitial water in the PB lattice at higher potentials, explaining the need for half-cell conditioning prior to full cell testing [14].

The voltage profiles for the full cell can be seen in Fig. 7b, where cycling was performed at 50 mA $g^{-1}_{graphite}$ at various temperatures, resulting in a specific energy of 90 Wh kg^{-1} (calculated using both electrode masses) and a corresponding specific power of 25 W kg^{-1} (~C/4 discharge) at 22 °C. In comparison, commercial LIBs have a much higher specific energy of 150 Wh kg^{-1} and specific power of 50 W kg^{-1} (~C/3 discharge). This is due to the low capacity of KIB graphitic anode as well PB cathodes [58]. Notably, at 0 °C, a capacity of 100 mAh g^{-1} was achieved, in contrast to the negligible value obtained for graphite in the half-cell configuration. A 50% loss in capacity was observed going from room temperature to 0 °C, with an associated increase in cell hysteresis, albeit not to the extent observed in the half-cell. These results confirm the issues of using K metal as a counter electrode for half-cell testing for KIBs. Long term cycling of this full cell, as shown in Fig. 7c, results in a capacity retention of 50% from cycle 3 to 50, which can be attributed to the poor Coulombic efficiency (< 96%). Upon inspection of the cell after cycling, the electrolyte had turned a dark color, likely due to side reactions at high potentials and the release of water in PB cathode, resulting in a rise in cell impedance over time. This study indicates that while KIBs have shown promise in optimal conditions in the prior literature, there remains much improvement to be made in terms of cycling stability and performance, especially at non-ideal conditions.

4. Conclusions

For the first time in the literature, we have investigated the temperature dependent behavior of KIBs, specifically with reference to the promising graphite anode. Comparisons between KIB and LIB electrochemical performance were made in terms of three categories, namely: rate capability, cell aging, and polarization. Notably, severe kinetic limitations are observed for KIBs at low temperatures, which can be

attributed to the increased solid-state diffusion activation energy, charge-transfer resistance, and SEI resistance. The solid-state diffusion coefficient for K^+ in graphite is two orders of magnitude smaller than that of Li (10^{-13} $cm^2 s^{-1}$ vs. 10^{-11} $cm^2 s^{-1}$), which can be attributed to the larger cationic size. While LIB graphite anode demonstrated good cycling stability at 40 °C, the KIBs exhibited accelerated capacity fade with increasing temperature, due to continuous SEI growth and impedance rise. Evaluation of K metal as the counter electrode revealed extreme polarization at low temperatures (161 mV at 0 °C at 20 mA g^{-1}) and poor stability at elevated temperatures due to dramatic electrolyte breakdown. Full-cell evaluation using graphite anode and Prussian blue cathode revealed enhanced performance at low temperatures, elucidating the issues of K metal for KIB electrode evaluation. These results provide valuable mechanistic insight into graphite anode for KIBs, providing a practical evaluation of the temperature dependent electrochemical performance and the K metal counter electrode used to study KIB performance.

Acknowledgements

We thank the National Science Foundation for supporting our potassium ion battery safety work under the CBET-1804300 grant. VP thanks the Office of Naval Research for supporting lithium ion battery safety work under the grant N00014-18-1-2397. RA acknowledges the Bilsland Dissertation Fellowship for financial support, as well as Arthur Dysart for his helpful discussions regarding electrochemical impedance spectroscopy analysis.

Appendix A. Supplementary data

Experimental details about the diffusion coefficient calculation, Prussian blue cathode, and full cell preparation are included; electrochemical impedance spectroscopy fitting parameters and Nyquist plots are shown; GITT profiles and additional electrochemical testing figures are included.

Supplementary data to this article can be found online at https://doi.org/10.1016/j.jpowsour.2018.11.007.

References

[1] J.-M. Tarascon, Nat. Chem. 2 (2010), https://doi.org/10.1038/nchem.680 510–510.
[2] D. Larcher, J.-M. Tarascon, Nat. Chem. 7 (2015) 19–29, https://doi.org/10.1038/nchem.2085.
[3] Y. Guo, Y. Li, X. Lou, J. Guan, Y. Li, X. Mai, H. Liu, C.X. Zhao, N. Wang, C. Yan, G. Gao, H. Yuan, J. Dai, R. Su, Z. Guo, J. Mater. Sci. 53 (2018) 13790–13800, https://doi.org/10.1007/s10853-018-2229-0.
[4] J. Guan, H. Xiao, X. Lou, Y. Guo, X. Luo, Y. Li, C. Yan, X. Yan, G. Gao, H. Yuan, J. Dai, R. Su, W. Gu, Z. Guo, ES Energy Environ (2018) 1–26, https://doi.org/10.30919/esee8c126.
[5] K. Kubota, S. Komaba, J. Electrochem. Soc. 162 (2015) A2538–A2550, https://doi.org/10.1149/2.0151514jes.
[6] X. Wu, D.P. Leonard, X. Ji, Chem. Mater. 29 (2017) 5031–5042, https://doi.org/10.1021/acs.chemmater.7b01764.
[7] K. Kubota, M. Dahbi, T. Hosaka, S. Kumakura, S. Komaba, Chem. Rec. 18 (2018) 459–479, https://doi.org/10.1002/tcr.201700057.
[8] H. Kim, J.C. Kim, M. Bianchini, D.-H. Seo, J. Rodriguez-Garcia, G. Ceder, Adv. Energy Mater. 8 (2018) 1702384, https://doi.org/10.1002/aenm.201702384.
[9] A. Eftekhari, Z. Jian, X. Ji, ACS Appl. Mater. Interfaces 9 (2017) 4404–4419, https://doi.org/10.1021/acsami.6b07989.
[10] C. Vaalma, G.A. Giffin, D. Buchholz, S. Passerini, J. Electrochem. Soc. 163 (2016) A1295–A1299, https://doi.org/10.1149/2.0921607jes.
[11] X. Wang, X. Xu, C. Niu, J. Meng, M. Huang, X. Liu, Z. Liu, L. Mai, Nano Lett. 17 (2017) 544–550, https://doi.org/10.1021/acs.nanolett.6b04611.
[12] H. Kim, J.C. Kim, S.-H. Bo, T. Shi, D.-H. Kwon, G. Ceder, Adv. Energy Mater. 7 (2017) 1700098, https://doi.org/10.1002/aenm.201700098.
[13] K. Chihara, A. Katogi, K. Kubota, S. Komaba, Chem. Commun. 53 (2017) 5208–5211, https://doi.org/10.1039/C6CC10280H.
[14] C. Zhang, Y. Xu, M. Zhou, L. Liang, H. Dong, M. Wu, Y. Yang, Y. Lei, Adv. Funct. Mater. 27 (2017) 1604307, https://doi.org/10.1002/adfm.201604307.
[15] L. Xue, Y. Li, H. Gao, W. Zhou, X. Lü, W. Kaveevivitchai, A. Manthiram, J.B. Goodenough, J. Am. Chem. Soc. 139 (2017) 2164–2167, https://doi.org/10.1021/jacs.6b12598.
[16] X. Bie, K. Kubota, T. Hosaka, K. Chihara, S. Komaba, J. Mater. Chem. 5 (2017) 4325–4330, https://doi.org/10.1039/C7TA00220C.
[17] Z. Jian, Z. Xing, C. Bommier, Z. Li, X. Ji, Adv. Energy Mater. 6 (2016) 1501874, https://doi.org/10.1002/aenm.201501874.
[18] R.A. Adams, J.-M. Syu, Y. Zhao, C.-T. Lo, A. Varma, V.G. Pol, ACS Appl. Mater. Interfaces 9 (2017) 17872–17881, https://doi.org/10.1021/acsami.7b02476.
[19] Y. Li, R.A. Adams, A. Arora, V.G. Pol, A.M. Levine, R.J. Lee, K. Akato, A.K. Naskar, M.P. Paranthaman, J. Electrochem. Soc. 164 (2017) A1234–A1238, https://doi.org/10.1149/2.1391706jes.
[20] X. Wang, K. Han, D. Qin, Q. Li, C. Wang, C. Niu, L. Mai, Nanoscale 9 (2017) 18216–18222, https://doi.org/10.1039/C7NR06645G.
[21] M. Naguib, R.A. Adams, Y. Zhao, D. Zemlyanov, A. Varma, J. Nanda, V.G. Pol, Chem. Commun. 53 (2017) 6883–6886, https://doi.org/10.1039/C7CC02026K.
[22] Z. Wang, A.P. Ratvik, T. Grande, S.M. Selbach, RSC Adv. 5 (2015) 15985–15992, https://doi.org/10.1039/C4RA15529G.
[23] Z. Jian, W. Luo, X. Ji, J. Am. Chem. Soc. 137 (2015) 11566–11569, https://doi.org/10.1021/jacs.5b06809.
[24] S. Komaba, T. Hasegawa, M. Dahbi, K. Kubota, Electrochem. Commun. 60 (2015) 172–175, https://doi.org/10.1016/j.elecom.2015.09.002.
[25] W. Luo, F. Shen, C. Bommier, H. Zhu, X. Ji, L. Hu, Acc. Chem. Res. 49 (2016) 231–240, https://doi.org/10.1021/acs.accounts.5b00482.
[26] J. Zhao, X. Zou, Y. Zhu, Y. Xu, C. Wang, Adv. Funct. Mater. 26 (2016) 8103–8110, https://doi.org/10.1002/adfm.201602248.
[27] M.T.F. Rodrigues, G. Babu, H. Gullapalli, K. Kalaga, F.N. Sayed, K. Kato, F.N. Sayed, K. Kato, J. Joyner, P.M. Ajayan, Nat. Energy. 2 (2017) 17108, https://doi.org/10.1038/nenergy.2017.108.
[28] S. Zhang, K. Xu, T. Jow, Electrochim. Acta 48 (2002) 241–246, https://doi.org/10.1016/S0013-4686(02)00620-5.
[29] M. Petzl, M. Kasper, M.A. Danzer, J. Power Sources 275 (2015) 799–807, https://doi.org/10.1016/j.jpowsour.2014.11.065.
[30] M.D. Levi, C. Wang, J.S. Gnanaraj, D. Aurbach, J. Power Sources 119–121 (2003) 538–542, https://doi.org/10.1016/S0378-7753(03)00279-9.
[31] T. Waldmann, M. Wilka, M. Kasper, M. Fleischhammer, M. Wohlfahrt-Mehrens, J. Power Sources 262 (2014) 129–135, https://doi.org/10.1016/j.jpowsour.2014.03.112.
[32] Q. Wang, P. Ping, X. Zhao, G. Chu, J. Sun, C. Chen, J. Power Sources 208 (2012) 210–224, https://doi.org/10.1016/j.jpowsour.2012.02.038.
[33] R.A. Adams, A. Varma, V.G. Pol, J. Power Sources 375 (2018) 131–137, https://doi.org/10.1016/j.jpowsour.2017.11.065.
[34] D. Juarez-Robles, C.-F. Chen, Y. Barsukov, P.P. Mukherjee, J. Electrochem. Soc. 164 (2017) A837–A847, https://doi.org/10.1149/2.1251704jes.
[35] R. Gnanamuthu, C.W. Lee, Mater. Chem. Phys. 130 (2011) 831–834, https://doi.org/10.1016/j.matchemphys.2011.08.060.
[36] C.-K. Huang, J.S. Sakamoto, J. Wolfenstine, S. Surampudi, J. Electrochem. Soc. 147 (2000) 2893, https://doi.org/10.1149/1.1393622.
[37] S. Müller, J. Eller, M. Ebner, C. Burns, J. Dahn, V. Wood, J. Electrochem. Soc. 165 (2018) A339–A344, https://doi.org/10.1149/2.0311802jes.
[38] T.L. Kulova, A.M. Skundin, Russ. J. Electrochem. 42 (2006) 251–258, https://doi.org/10.1134/S1023193506030074.
[39] T.L. Kulova, A.M. Skundin, E.A. Nizhnikovskii, A.V. Fesenko, Russ. J. Electrochem. 42 (2006) 259–262, https://doi.org/10.1134/S1023193506030086.
[40] P. Yu, J. Electrochem. Soc. 146 (1999) 8, https://doi.org/10.1149/1.1391556.
[41] K. Nobuhara, H. Nakayama, M. Nose, S. Nakanishi, H. Iba, J. Power Sources 243 (2013) 585–587, https://doi.org/10.1016/j.jpowsour.2013.06.057 Short communication.
[42] S.S. Zhang, K. Xu, T.R. Jow, Electrochim. Acta 49 (2004) 1057–1061, https://doi.org/10.1016/j.electacta.2003.10.016.
[43] K. Xu, Y. Lam, S.S. Zhang, T.R. Jow, T.B. Curtis, J. Phys. Chem. C 111 (2007) 7411–7421, https://doi.org/10.1021/jp068691u.
[44] M. Steinhauer, S. Risse, N. Wagner, K.A. Friedrich, Electrochim. Acta 228 (2017) 652–658, https://doi.org/10.1016/j.electacta.2017.01.128.
[45] M. Hess, J. Electrochem. Soc. 165 (2018) A323–A332, https://doi.org/10.1149/2.0701802jes.
[46] E. de la Llave, V. Borgel, E. Zinigrad, F.-F. Chesneau, P. Hartmann, Y.-K. Sun, D. Aurbach, Isr. J. Chem. 55 (2015) 1260–1274, https://doi.org/10.1002/ijch.201500064.
[47] T.A. Pham, K.E. Kweon, A. Samanta, V. Lordi, J.E. Pask, J. Phys. Chem. C 121 (2017) 21913–21920, https://doi.org/10.1021/acs.jpcc.7b06457.
[48] Y. Chen, L. Shi, A. Li, S. Zhang, M. Guo, X. Chen, J. Zhou, H. Song, J. Electrochem. Soc. 164 (2017) A2000–A2006, https://doi.org/10.1149/2.1151709jes.
[49] D. Abraham, R. Twesten, M. Balasubramanian, I. Petrov, J. McBreen, K. Amine, Electrochem. Commun. 4 (2002) 620–625, https://doi.org/10.1016/S1388-2481(02)00388-0.
[50] W. Waag, S. Käbitz, D.U. Sauer, Appl. Energy 102 (2013) 885–897, https://doi.org/10.1016/j.apenergy.2012.09.030.
[51] Q. Liu, C. Du, B. Shen, P. Zuo, X. Cheng, Y. Ma, G. Yin, Y. Gao, RSC Adv. 6 (2016) 88683–88700, https://doi.org/10.1039/C6RA19482F.
[52] N. Xiao, W.D. McCulloch, Y. Wu, J. Am. Chem. Soc. 139 (2017) 9475–9478, https://doi.org/10.1021/jacs.7b04945.
[53] M. Hess, Electrochim. Acta 244 (2017) 69–76, https://doi.org/10.1016/j.electacta.2017.05.017.
[54] R. Yazami, Y. Reynier, Electrochim. Acta 47 (2002) 1217–1223, https://doi.org/10.1016/S0013-4686(01)00827-1.
[55] T. Utsunomiya, O. Hatozaki, N. Yoshimoto, M. Egashira, M. Morita, J. Power Sources 196 (2011) 8598–8603, https://doi.org/10.1016/j.jpowsour.2011.05.066.
[56] Y. Lei, L. Qin, R. Liu, K.C. Lau, Y. Wu, D. Zhai, B. Li, F. Kang, ACS Appl. Energy Mater. 1 (2018) 1828–1833, https://doi.org/10.1021/acsaem.8b00214.
[57] W. Zhang, W.K. Pang, V. Sencadas, Z. Guo, Joule. (2018) 1–14. doi:10.1016/j.joule.2018.04.022.
[58] Electrochemical Energy Storage Technical Team Roadmap, (2017) https://www.energy.gov/sites/prod/files/2017/11/f39/EESTTroadmap2017-10-16Final.pdf.